Scattering analysis of arbitrarily shaped cylinders in a focused beam system-oblique incidence case

R. Shavit, J. Sangiolo and T. Monk

Abstract: The scattering from an arbitrarily shaped cylinder for the general oblique incident case is characterised by its induced field ratio (IFR) and its co-polarised and cross-polarised scattering patterns. The paper describes how a unique focused-beam measurement system is used to determine experimentally the scattering characteristics of an arbitrarily shaped cylinder for an obliquely incident plane wave. The fields of the transmitting and receiving antennas of the focused-beam measurement system are approximated by equivalent fundamental Gaussian beams. An analytical algorithm, based on computation of the coupling between the transmit and receive Gaussian beams of the focused-beam measurement system and the scattered field of the cylinder, is used to determine the IFR and the co-polarised and cross-polarised scattering patterns of the cylinder. The experimental results obtained by this method for typical dielectric and metal cylinders agree well with the theoretical scattering characteristics computed numerically by the method of moments (MOM) and the finite element method (FEM).

1 Introduction

Accurate characterisation of the scattering properties of dielectric and metal beams is essential in the electromagnetic analysis of large sandwich and dielectric/metal space frame radomes assembled from a large number of beams or panels. These beam or panel joints introduce scattering effects that modify the radiation characteristics of the antenna enclosed in the radome.

The total scattering effect of the radome can be evaluated as the summation of the scattered fields from all beam or panel joints illuminated by the antenna (in a transmit mode analysis). The fundamental basis for such a computation is the knowledge of the scattering characteristics from an individual beam located and oriented at a specified point in space and illuminated by a plane wave propagating in a particular direction. Therefore the ability to compute and measure the scattering characteristics of an arbitrarily shaped cylinder is essential to the entire scattering analysis.

Kay [1] was the first to introduce the concepts of induced field ratio (IFR) and scattering pattern to characterise the scattering effect of the beams on the metal space frame radome electromagnetic performance. The IFR is defined as the ratio of the forward scattered field to the hypothetical field radiated in the forward direction by the plane wave in the reference aperture of width equal to the shadow of the geometrical cross-section of the cylinder on the incident wavefront [2]. Low values of IFR are indicative of low scattering effect in the forward direction.

In his analysis, Kay [1] disregarded the cross-polarised scattering from the beams and neglected the variation of the co-polarised scattering pattern for obliquely incident plane waves. This missing information can be recovered using the suggested experimental method. The full scattering analysis for an arbitrarily shaped dielectric beam illuminated by an oblique incident plane wave was first formulated by Rojas [3]. The analysis shows the existence of cross-polarised scattering for oblique incident angles, absent at normal incidence.

Analytical computations of the scattering characteristics for cylinders can be performed for canonical cross-sections, such as circles and ellipses, but, for arbitrarily shaped cylinders, numerical computations using techniques such as the method of moments (MOM) [4] and the finite element method (FEM) [5] are required.

These numerical techniques are, in many cases, numerically intensive. Consequently, in many practical instances, to reduce development cycle times, control manufacturing processes and verify numerical predictions, an accurate method of experimentally determining the IFR and scattering patterns (both co-polarised and cross-polarised) of the cylinder is required.

Rusch [2] developed the IFR concept and suggested an experimental procedure to measure its value in the far-field for an arbitrarily shaped cylinder. This procedure lacks the capability to measure the scattering pattern and lacks the ability to filter out the reflections from surrounding objects, which compromise the accuracy of the measurement.

An alternative experimental approach using a focused-beam measurement system has been analysed in [6] and improved in [7] using a Gabor representation. The unique characteristics of the focused-beam measurement system provide a tightly constrained field distribution at the beam waist, normally midway between the transmitting and receiving ends, which facilitates the separation of the incident field from the scattered field by a cylinder inserted in such a system at the beam waist. This feature improves significantly the accuracy of the measured scattering

IEE Proc.-Microw. Antennas Propag., Vol. 148, No. 2, April 2001

73

parameters of the tested cylinder. Moreover, this new method also provides a reduction in the measurement errors associated with specular and diffuse reflections from scatterers in the vicinity of the test facility present in previous measurement systems [2].

The current paper extends the scattering analysis of an arbitrarily shaped cylinder, measured in a focused-beam system for normal incidence and described in [6, 7], to the oblique incident case. The analysis presented extracts the IFR and the co-polarised/cross-polarised scattering patterns of the cylinder, which is a unique feature of this method. In addition, the paper verifies the accuracy of the results obtained using the suggested method against computed numerical results obtained by the MOM and the FEM. This information improves the computation accuracy of the scattering analysis presented by Kay [1] for metal/dielectric space frame radomes.

2 Method description

A schematic form of the focused-beam measurement system is shown in Fig. 1. The system comprises two identical, axially symmetric, dielectric lenses L_1 and L_2, with aperture diameter D, and two identical, linearly polarised feed horns H_1 and H_2. Each lens is designed so that its two foci are located at distances f_1 and f_2 from the lens surface on opposite sides of the lens. The distance of the feed horn phase centre from the lens surface is d_1.
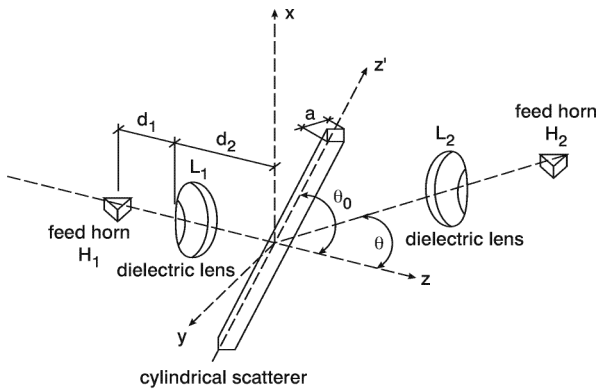

Fig. 1 *Schematic configuration of focused-beam system*

In principle, the system is configured such that $f_1 = d_1$; however, owing to movement of the feed horn phase centre with frequency and the fact that the location of the Gaussian beam waist on the other side of the lens is frequency dependent, this requirement is not perfectly achieved at all frequencies.

The energy radiated by the transmitting feed horn H_1 is captured by the lens L_1, and is focused on the opposite side of the lens to the common focal point of the two lenses, at a distance d_2 from the lens surface, coupled to the receiving lens L_2 and re-focused into the feed horn H_2. Accordingly, feed horn H_1 and lens L_1 are designated as the transmitting antenna, and feed horn H_2 and lens L_2 are designated as the receiving antenna. The focal plane of the system is defined as the plane passing through the internal (common) focal point of the two lenses, perpendicular to the system axis. This plane also represents the approximate location of the beam waists of the Gaussian beams of the two antenna systems. In the measurement to be described, the centre of the cylindrical scatterer is located in this focal plane, and its axis makes an angle θ_0 with the system axis, as shown in Fig. 1.

The assumption is made that the propagation mechanism of the focused-beam system can be described by fundamental Gaussian beams [8]. Accordingly, the divergent Gaussian beam of the transmit feed horn H_1 (see Fig. 1) is transformed by the transmitting lens to a convergent Gaussian beam with minimum waists w_{0x} and w_{0y} in the internal focal plane. By considerations of symmetry, the convergent Gaussian beam is transformed into a divergent Gaussian beam captured by the receiving lens and subsequently transformed into a convergent Gaussian beam captured by the receiving feed horn H_2. In the internal focal plane, we obtain a minimum Gaussian beam waist with constant phase distribution.

Initially, before the cylinder is moved into the focal plane, the co-polarised coupling between the two focused-beams is recorded (amplitude and phase) to provide a reference value. The tested cylinder is then positioned in the focal plane and inclined at an angle θ_0 relative to the system axis, and the coupling between the two focused-beams normalised to the no-cylinder case $R(y) = \Delta\alpha \ e^{j\Delta\phi}$ recorded ($\Delta\alpha$ is the relative amplitude, and $\Delta\phi$ is the relative phase). Then, the receiving lens L_2 and its feeding horn H_2 are rotated in predetermined angular increments on an arch with its centre of rotation located in the focal plane. For each angular point, two readings are taken, with and without the cylinder. The procedure is repeated for the cross-polarised case with the receiving feed horn H_2 rotated 90° around its axis.

2.1 System analysis without the scatterer
The angular dependence of the co-polarised transmission loss between the two antennas is proportional to the coupling between the inward and outward Gaussian beams in the focal plane, as shown in [8]. The co-polarised electric field distribution of the inward Gaussian beam in the focal plane ($z = 0$) is described in [8] by

$$f^t_{copol} e^{-\frac{x^2}{w_{0x}^2} - \frac{y^2}{w_{0y}^2}}$$

in which $f^t_{copol} = $ const. In a similar fashion, the cross-polarised term can be described by

$$f^t_{xpol}(y) e^{-\frac{x^2}{w_{0x}^2} - \frac{y^2}{w_{0y}^2}}$$

for a $\underline{1}_x$ polarised electric field. Accordingly, the total electric field distribution of the inward Gaussian beam in the focal plane can be described by

$$\underline{f}^t(x,y) = (f^t_{copol}\underline{1}_x + f^t_{xpol}(y)\underline{1}_y) e^{-\frac{x^2}{w_{0x}^2} - \frac{y^2}{w_{0y}^2}} \quad (1)$$

where f^t_{copol} and f^t_{xpol} (y) are determined by the co-polarised and cross-polarised characteristics of the feed horn H_1 and the lens L_1. In most cases, $f^t_{copol} >> f^t_{xpol}$. The electric field distribution of the outward Gaussian beam in the focal plane $f^r(x, y)$ can be expressed in a similar fashion, but with the addition of a linear progressive phase, owing to the non-alignment of this beam with the system axis (see Fig. 1)

$$\underline{f}^r(x,y) = (f^r_{copol}\underline{1}_x + f^r_{xpol}(y)\underline{1}_y) e^{-\frac{x^2}{w_{0x}^2} - \frac{y^2}{w_{0y}^2}} e^{-jky\sin\theta}$$

$$(2)$$

Owing to the symmetry of the system, it can be assumed that $f^t_{copol} = f^r_{copol} = f^t_0$ and $f^t_{xpol} = f^r_{xpol}$. The coupling factor $C_c(\theta)$ between the two beams in the focal plane is computed by performing a two-dimensional integral in the focal plane over the scalar product of the two electric field distributions, $f^t(x, y)$ and $f^r(x, y)$ as described in [8]. This exercise results in a co-polarised coupling factor C^c_{copol} (θ) and a cross-polarised coupling factor C^c_{xpol} (θ). Using sepa-

74

IEE Proc.-Microw. Antennas Propag., Vol. 148, No. 2, April 2001

ration of variables, the integration over x can be performed analytically, and the result can be absorbed in f_0^t. Thus the simplified co-polarised coupling factor $C_{copol}^c(\theta)$ is given by

$$C_{copol}^c(\theta) = \int_{-\infty}^{\infty} \underline{f^t} \cdot \underline{f^{r*}} \, dy$$

$$\cong \left| f_0^t \right|^2 \int_{-\infty}^{\infty} e^{-\frac{2y^2}{w_{0y}^2}} \cdot e^{jky \sin\theta} dy \quad (3)$$

Evaluation of the integral results in

$$C_{copol}^c(\theta) = C_0 e^{-\frac{1}{2}\left(\frac{w_{0y}\pi}{\lambda}\sin\theta\right)^2} \quad C_0 = \left| f_0^t \right|^2 w_{0y}\sqrt{\pi/2} \quad (4)$$

The co-polarised coupling factor $C_{copol}^c(\theta)$ can be either computed through eqn. 4 or directly measured. In a similar fashion, the cross-polarised coupling factor $C_{xpol}^c(\theta)$ can be computed by

$$C_{xpol}^c(\theta)$$
$$= 2\text{Re}\left\{ \int_{-\infty}^{\infty} f_{copol}^t \cdot f_{xpol}^{t*}(y) e^{-\frac{2y^2}{w_{0y}^2}} e^{jky\sin\theta} dy \right\} \quad (5)$$

or directly measured, if the receiving feed horn H_2 is rotated by 90° around its axis.

2.2 System analysis with the scatterer

In this case, the cylinder scattered field $f^s(x, y)$ in the focal plane is added to the inward Gaussian beam, and the total field is coupled to the outward Gaussian beam of the receiving end. In a similar fashion to the assumption made in eqn. 1, the scattered field can be approximated by

$$\underline{f^s} =$$
$$\begin{cases} (f_{copol}^s(y)\underline{1}_x + f_{xpol}^s(y)\underline{1}_y) e^{-\frac{x^2}{w_{0x}^2} - \frac{y^2}{w_{0y}^2}} & |y| \leq \frac{a}{2} \text{ and } |x| < \infty \\ 0 & \text{elsewhere} \end{cases} \quad (6)$$

in which $f_{copol}^s(y)$ and $f_{xpol}^s(y)$ are the co-polarised and cross-polarised scattered electric fields in the focal plane ($z = 0$) for uniform plane wave illumination, and a is the projected width of the cylinder in the focal plane. $f_{copol}^s(y)$ and $f_{xpol}^s(y)$ are tapered by the exponential term owing to the Gaussian beam characteristics in the focal plane. In the co-polarised case, both feed horns at the transmit and receive ends are aligned, and we can neglect the cross-polarised contribution, as $f_{copol}^t \gg f_{xpol}^t$. The coupling factor in the focal plane $C_{copol}^t(\theta)$ between the total field in the vicinity of the cylinder

$$(f_{copol}^t + f_{copol}^s(y)) e^{-\frac{x^2}{w_{0x}^2} - \frac{y^2}{w_{0y}^2}}$$

and the outward Gaussian beam

$$f_{copol}^r e^{-\frac{x^2}{w_{0x}^2} - \frac{y^2}{w_{0y}^2}} e^{-jky\sin\theta}$$

is computed by performing a two-dimensional integration in the focal plane over the scalar product of the two electric field distributions, as described in [8]. Using separation of variables, the integration over x can be performed analytically and the result can be absorbed in both f_{copol}^t and $f_{copol}^s(y)$. Accordingly, the co-polarised coupling can be described by

$$C_{copol}^t(\theta) = \int_{-\infty}^{\infty} \left(f_{copol}^t(y) \right.$$
$$\left. + f_{copol}^s(y) \right) \cdot f_{copol}^{r*} e^{-\frac{2y^2}{w_{0y}^2}} e^{jky\sin\theta} dy \quad (7)$$

If we normalise both sides by C_0 (the value recorded at $\theta = 0$ without any scatterer) and substitute eqn. 3 into eqn. 7, we obtain

$$C_{copol}^t(\theta) - C_{copol}^c(\theta)$$
$$= f_0^{t*} \int_{-a/2}^{a/2} f_{copol}^s(y) e^{-\frac{2y^2}{w_{0y}^2}} e^{jky\sin\theta} dy \quad (8)$$

All quantities on the left-hand side of eqn. 8 are either analytically computable or directly measurable. Moreover, if we recall [9] that the scattering radiation pattern $E_{copol}^s(\theta)$ for uniform plane wave illumination can be computed by

$$E_{copol}^s(\theta) = \int_{-a/2}^{a/2} f_{copol}^s(y) e^{jky\sin\theta} dy \quad (9)$$

and compare the $E_{copol}^s(\theta)$ expression with the right-hand side (RHS) of eqn. 8, we can recognize that the RHS of eqn. 8 is the co-polarised scattering pattern of a tapered scattered field distribution in the focal plane. Thus $E_{copol}^s(\theta)$ for uniform plane wave illumination can be reconstructed from the data in eqn. 8, either by applying an FFT algorithm [6] or by using Gabor basis functions to express $f_{copol}^s(y)$, as described in [7].

The cross-polarised coupling factor is obtained if the feed horn at the receiving end is rotated 90° around its axis. In a similar fashion to the co-polarised case, the cross-polarised coupling factor $C_{xpol}^t(\theta)$, between the co-polarised total field in the vicinity of the cylinder and the cross-polarised field of the outward Gaussian beam of the receiving end, can be expressed by

$$C_{xpol}^t(\theta) = C_{xpol}^c(\theta) + \int_{-a/2}^{a/2} \left(f_{copol}^s(y) \cdot f_{xpol}^{r*}(y) \right.$$
$$\left. + f_{xpol}^s(y) \cdot f_{copol}^{r*}(y) \right) e^{-\frac{2y^2}{w_{0y}^2}} e^{jky\sin\theta} dy \quad (10)$$

Eqn. 10 can be simplified if the assumption that $f_{copol}^s(y) = \text{const} = f_0^s$ is made on the scatterer surface in the focal plane ($z = 0$). In this case, the co-polarised scattered field f_0^s can be evaluated from eqn. 8, for $\theta = 0$, to be

$$\frac{f_0^s}{f_0^t} = \left(\frac{C_{copol}^t(0)}{C_0} - 1 \right) \frac{1}{erf\left(\frac{a}{\sqrt{2}w_{0y}}\right)} \quad (11)$$

in which $erf(x) = 2/\sqrt{(\pi)}\int_0^x e^{-t^2}dt$. Substitution of eqn. 11 into eqn. 10 yields

$$C_{xpol}^t(\theta) - C_{xpol}^c(\theta)$$
$$- \frac{f_0^s}{f_0^t} \int_{-a/2}^{a/2} f_{xpol}^{r*}(y) e^{-\frac{2y^2}{w_{0y}^2}} e^{jky\sin\theta} dy$$
$$= \int_{-a/2}^{a/2} f_{xpol}^s(y) e^{-\frac{2y^2}{w_{0y}^2}} e^{jky\sin\theta} dy \quad (12)$$

All quantities involved on the LHS of eqn. 12 are either directly measured, such as $C_{xpol}^t(\theta)$, $C_{xpol}^c(\theta)$, $f_{xpol}^r(y)$, or

computable. Similar considerations for the co-polarised case lead us to recognise that the RHS of eqn. 12 is proportional to the cross-polarised scattering pattern of a tapered cross-polarised scattered field distribution in the focal plane, with $\exp(-2y^2/w_{0y}^2)$ being the tapering factor. The correct cross-polarised scattering pattern $E_{xpol}^s(\theta)$ can be reconstructed from the data in eqn. 12, by applying an FFT algorithm in a similar fashion to the procedure described in the co-polarised case.

2.3 IFR computation for the oblique case

The IFR_E (co-polarised TM case) of an arbitrarily shaped cylinder for normal incidence is given by [2]

$$IFR_E = -\frac{Z_0}{2aE_0} \int_s J_{sz'} e^{jk\rho' \sin\phi'} dl \qquad (13)$$

in which $Z_0 = \sqrt{(\mu_0/\varepsilon_0)} \cong 120\pi\,\Omega$ is the characteristic impedance of free space (μ_0 and ε_0 are the permeability and permittivity of free space), $J_{sz'}$ is the axial induced current distribution on the cylinder, and E_0 is the intensity of the incident electric field. The extension of eqn. 12 to the oblique incidence case would be

$$IFR_E = -\frac{Z_0 \sin\theta_0}{2aE_0} \int_s J_{sz'} e^{jk\rho' \sin\theta_0 \sin\phi'} dl \quad (14)$$

Similarly, for the TE case, the IFR_H would be

$$IFR_H = -\frac{\sin\theta_0}{2aH_0} \int_s H_{z'}(\mathbf{1}_z \cdot \mathbf{1}_n) e^{jk\rho' \sin\theta_0 \sin\phi'} dl \qquad (15)$$

in which $H_{z'}$ is the total axial magnetic field at the surface of the cylinder, and $\mathbf{1}_n$ is the unit vector normal to the cylinder surface. An alternative representation [6], valid for both TM and TE cases of the IFR that are derived in terms of the respective scattered electric field $f_{copol}^s(y)$ in the focal plane, is

$$IFR_{E,H} = (10^{\frac{\Delta\alpha}{20}} e^{j\Delta\phi} - 1)$$

$$\times \sqrt{\frac{\pi}{2}} \frac{w_{0y}}{a} \frac{\int_{-a/2}^{a/2} f_{copol}^s(y)dy}{\int_{-a/2}^{a/2} f_{copol}^s(y)e^{-\frac{2y^2}{w_{0y}^2}} dy} \qquad (16)$$

3 Numerical results

The measurements were performed on the focused-beam system described in [6], which is shown in Fig. 2. The diameter of the lenses on both receiving and transmitting ends was 55.9cm, and their focal distances f_1 and f_2 were 53.3cm and 203.2cm, respectively. At the operating frequency of 12GHz, the Gaussian beam waist sizes w_{0x} and w_{0y} in the focal plane were measured to be 6.54cm and 6.78cm, respectively, at -8.7dB points (the field is e^{-1} of its value on the axis).

Two rectangular cylinders (metal and dielectric) used in typical metal and dielectric space frame radomes were chosen for the theoretical verification. The cross-section of the metal cylinder was 1.37×5.16cm, and that of the dielectric cylinder was 1.19×5.69cm, with $\varepsilon_r = 5.0$. The cylinders were tested (co-polarised and cross-polarised) at 12GHz for both vertical (VP) and horizontal (HP) polarisations and for four oblique incident angles on their broadside. Owing to the physical constraints of the measurement setup, the angular extent of the focused-beam was $\theta_{max} = 70°$.
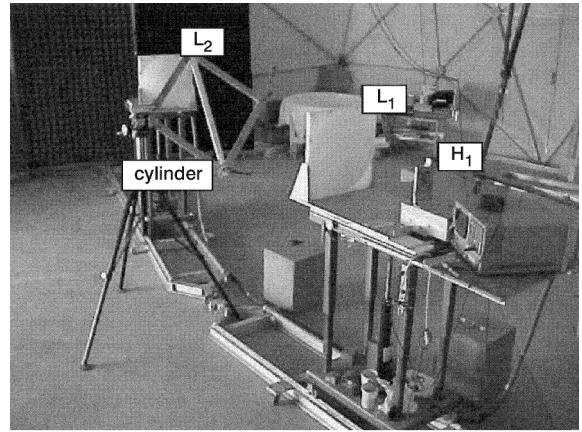

Fig. 2 *Focused-beam system of L-3 Communications-ESSCO, Concord, MA, USA*

The algorithm assumes that the cylinder is infinite in length, and therefore, to avoid any error caused by its finite length, it is chosen to be longer than $4w_{0x}/\sin\theta_0$. Such a choice makes the finite length of the cylinder irrelevant, as, for this case, the top and bottom of the cylinder are almost not illuminated (-34dB down). Accordingly, for practical reasons, this bound makes the method less attractive for small inclination angles θ_0 (see Fig. 1).

Initially, direct measurements of the co-polarised $f_{copol}^t(y)$ and cross-polarised $f_{xpol}^t(y)$ field distributions without the scatterer were performed in the focal plane at 12GHz using a small feed horn. Figs. 3 and 4 show the co-polarised and cross-polarised amplitude and phase distribution, respectively, in the focal plane for vertical polarisation. The comparison of the measured co-polarised data with the computed results using the assumption made in eqn. 1 shows a good agreement. We can observe that the maximum cross-polarised level (measured) owing to the lens L_1 and feed horn H_1 is less than -25dB. This information was stored in the computer for further processing.
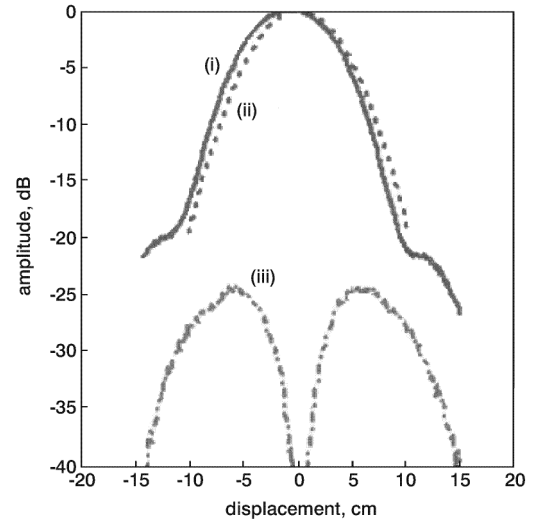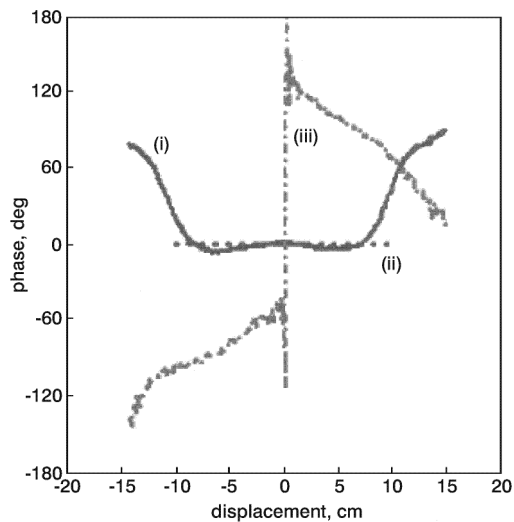

Fig. 3 *Measured amplitude distribution (co-polarised and cross-polarised) in focal plane for vertical polarisation*
(i) copol (measured)
(ii) copol (computed)
(iii) xpol (measured)

Figs. 5 and 6 show a typical recorded signal (amplitude and phase, respectively) for both co-polarised and cross-polarised measurements throughout the angular movement of the receiving end (horn H_2 and lens L_2) with the dielectric cylinder inclined by 30° ($\theta_0 = 60°$). The beam is illuminated by a vertical polarised wave on its broadside.

76

IEE Proc.-Microw. Antennas Propag., Vol. 148, No. 2, April 2001

Fig. 4 *Measured phase distribution (co-polarised and cross-polarised) in focal plane for vertical polarisation*
(i) copol (measured); (ii) copol (computed); (iii) xpol (measured)
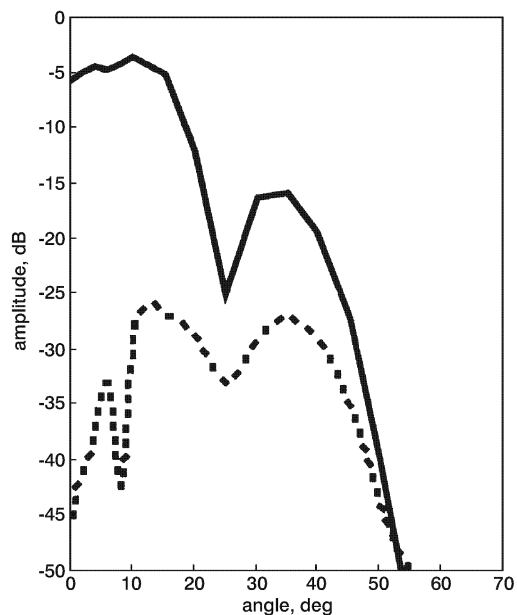
Fig. 5 *Amplitude of recorded signal for co-polarised and cross-polarised measurements with dielectric cylinder inclined by 30° (θ_0 = 60°) in focal plane, illuminated on its broadside at 12GHz with vertical polarisation*
——— copol; ········· xpol
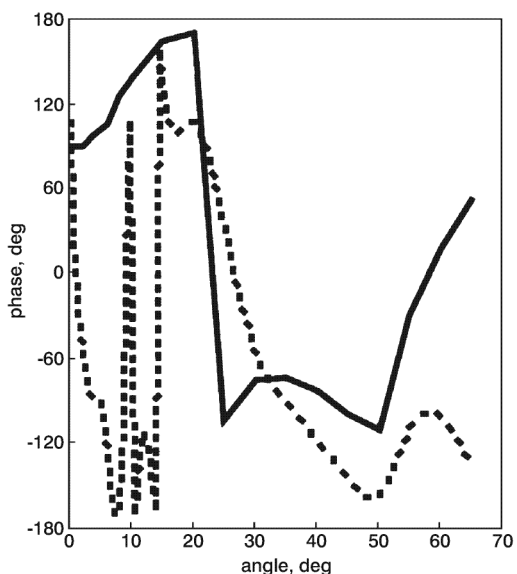
Fig. 6 *Phase of recorded signal for co-polarised and cross-polarised measurements with dielectric cylinder inclined by 30° (θ_0 = 60°) in focal plane, illuminated on its broadside at 12GHz with vertical polarisation*
——— copol; ········· xpol

The co-polarised recorded data (with and without the scatterer) were plugged in eqn. 8 and processed with an FFT algorithm to evaluate the tapered and corrected field distributions of the scatterer in the focal plane, $f^{s}_{copol}(y)$ as described in [6]. The next step was to compute the reconstructed, co-polarised radiation pattern of the scatterer using eqn. 9.

The cross-polarised recorded data (with and without the scatterer) were plugged in eqn. 12, and the cross-polarised scattered radiation pattern was computed. Fig. 7 shows the comparison between the computed scattering pattern (co-polarised and cross-polarised) obtained by FEM and the reconstructed scattering pattern (co-polarised and cross-polarised) using the recorded measured data in the focused-beam system.
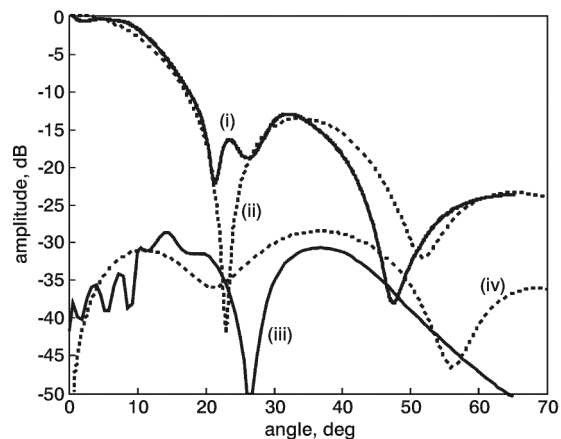
Fig. 7 *Comparison between computed (FEM) and reconstructed scattering patterns (co-polarised and cross-polarised) of dielectric cylinder inclined by 30° (θ_0 = 60°) in focal plane, illuminated on its broadside at 12GHz with vertical polarisation*
(i) reconstructed (copol)
(ii) computed (copol)
(iii) reconstructed (xpol)
(iv) computed (xpol)

We can observe that a good agreement in the main beam and in the sidelobe level is obtained, when we compare the computed and the reconstructed patterns. The ripple in the reconstructed pattern at $\theta \approx 23°$ is probably caused by corrupted phase measurement data amplified by the reconstruction algorithm. We can observe that the cross-polarised scattering pattern for oblique incident angles is significant and cannot be ignored in the scattering analysis of large space frame radomes. Moreover, it is interesting to note that the cross-polarised level in the direction of the incident field vanishes.

These observations confirm Rojas' [3] computational results, which predicted a significant cross-polarised scattering level of dielectric cylinders for oblique incident angles. This cross-polarised level vanishes completely for normal incidence on both metal and dielectric beams.

In addition, the data from all the measurements taken for both the dielectric and metal cylinders were processed to obtain the IFR_E and IFR_H based on eqn. 16 in the two-dimensional (2D) case. The results obtained were compared with the IFR values computed numerically by the MOM [4] for an infinite-length metallic cylinder (2D case) using two codes named ANYMFRE and ANYMFRH for TE and TM polarisations, respectively, and by FEM [5] for a dielectric cylinder (2D case) using a code named FEFD. All three codes were developed by the University of Illinois, Urbana, USA. Computation results of the IFR for four oblique incident angles at 12GHz are shown in Table 1.

We can observe a good agreement between the numerical computations (MOM and FEM) and the processed

Table 1: Comparison between measured and computed IFR values

Oblique incident angle, θ_0	Metal cylinder (α = 5.16cm)				Dielectric cylinder (α = 5.69cm)			
	computed (MOM)		measured		computed (FEM)		measured	
	IFR_E	IFR_H	IFR_E	IFR_H	IFR_E	IFR_H	IFR_E	IFR_H
90°	1.14∠172.6°	0.98∠−176.6	1.06∠172.4°	1.14∠−177.5	1.91∠163.8°	1.76∠167.1°	1.85∠159.0°	1.90∠166.9°
75°	1.15∠172.5°	N/A	1.1∠176.1°	1.2∠−178.1°	1.93∠161.7°	1.79∠165.0°	1.86∠157.9°	1.94∠164.1°
60°	1.15∠171.9°	N/A	1.12∠178.5°	1.3∠179.5°	1.99∠157.0°	1.86∠162.2°	1.93∠154.5°	2.06∠160.6°
45°	1.16∠170.2°	N/A	1.24∠−178.3°	1.26∠178.5°	2.02∠148.6°	1.79∠159.0°	1.93∠148.9°	1.91∠158.3°

measurement data acquired in the focused-beam system. It is interesting to note that the IFR variation with the incident angle is minor for both the IFR_E and IFR_H of the dielectric and metal cylinders. This observation justifies, to a certain extent, the original assumption made by Kay [1] in his co-polarised scattering analysis of the metal space frame radome, in which he neglected the variation of the IFR for different oblique incident angles and considered only the effect of the projected beams on the antenna surface in the radome enclosure.

4   Summary and conclusions

An extension to the oblique incident case (co-polarised and cross-polarised) of the scattering analysis and IFR computation of an arbitrarily shaped cylinder in a focused-beam system described in [6, 7] has been presented. The analysis is based on the assumption that the electric fields between the lenses can be described by fundamental Gaussian beams. The results obtained by the proposed method verify well the scattering characteristics computed analytically or numerically by the MOM and FEM. The focused-beam method complements Rusch's method. The information obtained on the scattering pattern (co-polarised and cross-polarised) helps to refine the calculations of the scattering analysis for large space frame radomes.

5   References

1   KAY, A.F.: 'Electrical design of metal space-frame radomes', *IEEE Trans.*, 1965, AP-13, pp. 188–202
2   RUSCH, W.V.T, HANSEN, J.A., KLEIN, C.A., and MITTRA, R.: 'Forward scattering from square cylinders in the resonance region with application to aperture blockage', *IEEE Trans.*, 1976, AP-24, pp. 182–189
3   ROJAS, R.G: 'Scattering by an inhomogeneous dielectric/ferrite cylinder of arbitrarily cross-section shape-oblique incidence case', *IEEE Trans.*, 1988, AP-36, pp. 238–246
4   RICHMOND, J.H.: 'Scattering by a dielectric cylinder of arbitrarily cross-section shape', *IEEE Trans.*, 1965, AP-13, pp. 334–341
5   JIN, J.: 'The finite element method in electromagnetics' (John Wiley & Sons, New York, 1993)
6   SHAVIT, R., WELLS, T., and COHEN, A.: 'Scattering analysis of arbitrarily shaped cylinders in a focused-beam system', *IEE Proc., Microw. Antennas Propag.,* 1998, 145, (4), pp. 284–289
7   SHAVIT, R.: 'Improved scattering analysis of arbitrarily shaped cylinders in a focused-beam system using Gabor representation', *IEE Proc., Microw. Antennas Propag.,* 1999, 146, (3), pp. 193–196
8   GOLDSMITH, P.F.: 'Infrared and millimeter waves' (Academic Press, New York, 1982)
9   ELLIOTT, R.S.: 'Antenna theory and design' (Prentice-Hall, New Jersey, 1981)

78

IEE Proc.-Microw. Antennas Propag., Vol. 148, No. 2, April 2001